ISSN: 2476- 2334

Research Article

International Journal of Nanotechnology & Nanomedicine

The Role of Roughness in Random Superhydrophobic Surfaces

T Nahum[1*], H Dodiuk[2], S Kenig[2], C Barry[1] and J Mead[1*]

[1]*Department of Plastics Engineering, University of Massachusetts Lowell, Lowell, MA 08154 USA*

[2]*Department of Polymers and Plastics Engineering, Shenkar College of Engineering Design and Art, Ramat Gan 52526, Israel*

[*]Corresponding author

Mead Joey, Department of Plastics Engineering, University of Massachusetts Lowell, Lowell, MA 08154 USA, E-mail: Joey_Mead@uml.edu

Submitted: 19 June 2018; **Accepted**: 22 June 2018; **Published**: 17 July 2018

Abstract

To investigate the role of roughness in superhydrophobic coatings a variety of superhydrophobic and non-superhydrophobic surfaces were synthesized using various polymer binders, nanosilica particles and fluoro chemistry on both glass and polycarbonate substrates. The roughness of the coatings was measured by profilometry and atomic force microscopy (AFM) and analyzed by a variety of statistical methods. Superhydrophobic surfaces showed a peak to peak distance below 5 microns and a radius of less than 0.5 micron, but this information alone was insufficient to predict superhydrophobicity. The skewness and kurtosis for the surfaces indicated that all coated samples, both superhydrophobic and non-superhydrophobic, had a random Gaussian roughness distribution, but there was no significant difference in the skewness and kurtosis values for either superhydrophobic or non-superhydrophobic surfaces. The power spectral density function (PSDF) was found to be an effective tool to predict the required roughness for superhydrophobicity and provides information over the entire range of length scales.

The average peak radius for the micro and nano scales calculated from ACL and RMS values were found to be less than 3 μm and 520 nm, respectively, which supports the accepted theory is that superhydrophobic surfaces require tightly packed asperities and small micron and nano roughness. The characterization of the surfaces allowed experimental verification of theoretical models for the roughness factor and critical roughness parameters. It was found that the RMS/ACL values should be 0.35 or higher for designing surfaces with contact angles above 150°. This work shows a unique method for measuring, quantifying, and understanding the role of roughness, that can be used to design surfaces for superhydrophobicity and future applications such as self-cleaning, icephobicity, anti-biofouling, corrosion resistance, and water repellency.

Keywords: superhydrophobic, roughness, nanoparticles, gaussian

Introduction

The level of interest in superhydrophobic surfaces, which are characterized by a contact angle (CA) above 150° and a sliding angle (SA) below 10°, has increased in the last decade due to their potential for use in applications such as self-cleaning, anti-corrosion, anti-fog, drag reduction, low water permeation, super-omniphobic surfaces and ice-repellency[1-22]. However, most of the state of the art superhydrophobic coatings lack durability, thus the development of a durable coating has been the subject of recent efforts [23-28].

Superhydrophobic surfaces are comprised of hierarchical roughness (micro and nano size) combined with hydrophobic chemistry. The hierarchical structure is needed for stability of trapped air and prevention of droplets from filling the valleys between the asperities and pinning the droplets [29]. However, the specific level of roughness required is still unresolved and different models have been proposed to optimize the level of roughness [30-34]. A few hierarchical structures have been suggested, among them circular pillars with diameter, D, height, H and pitch, P, and pyramidal nanoasperities with rounded tops [35]. The circular pillars should have dimensions at the interface, $(\sqrt{2}P - D)^2/R < H$, so the droplet droop is much smaller than the depth of the cavity and where the rounded nanoasperities should have a small pitch to handle nanodroplets (less than 1 mm down to a few nm radius). Later studies indicated that the specific surface texture of a ~3-μm-diameter pillar array with 7 μm height and different center to center spacings of 4.5, 6, 9, and 12 μm affected the wetting properties of the surface. In addition, nanopillars with aspect ratios of 2 and 5 with different spacings were shown to affect the contact angle [36]. It was also shown that superhydrophobicity can be obtained using flower-like sub-microsphere roughness, but also by micropillar arrays and micropyramid structures, when a hydrophobic nanostructure was added on top of the microstructures [37-42].

Predetermining the exact diameter, height or pitch is usually not applicable for engineering or natural surfaces, since the textures of most of these surfaces are random, either isotropic or anisotropic, and either Guassian or non-Gussian depending upon the processing method. In order to characterize the roughness of these surfaces several amplitude roughness parameters have been used [43]. The most common is the arithmetic average of the absolute values of the profile height deviations from the mean line, Ra, but this does

not give information about the shape or size of the roughness. It has been shown that different surface structures, both superhydrophobic and non-superhydrophobic, can have the same Ra value. Another parameter that is used to characterize surface roughness is the root mean square (RMS) value of the height fluctuations. A large value of the RMS indicates a rough surface and a small RMS indicates a smooth surface. The RMS, however, does not define the length scale parallel to the surface. Among the amplitude parameters such as Ra and RMS, skewness and kurtosis are also derived from the profile height distribution and give information about the height and shape of surface features (i.e., peaks and valleys). Skewness is the dimensionless measure of asymmetry of surface heights around the mean plane. A surface with positive skewness would be composed of "hills", while negative skewness corresponds to "valleys". Kurtosis is also a dimensionless measure of the shape of surface heights. A surface with high kurtosis exhibits spiky features, while a surface with low kurtosis shows more blunt topography. It was found that surfaces with high skewness and high kurtosis (values of 5.02 and 25.13, respectively), corresponding to a "spiky mountains" morphology, exhibited high contact angle and low hysteresis, whereas surfaces with negative skewness and low kurtosis (values of −1.27 and 7.36, respectively), represented a morphology similar to rounded valleys and displayed high contact angle, but high hysteresis [44].

Neither Ra, RMS, skewness, nor kurtosis provide information about the surface features in the horizontal direction. They characterize only roughness in the vertical direction perpendicular to the mean plane. To characterize the roughness in the horizontal direction of the surface, spatial functions are used. Among them are: autocorrelation function (ACF), structure function (SF), or power spectral density function (PSDF), which represent the wavelength distribution or spatial size of the features in the horizontal direction.

PSDF, which is the Fast Fourier Transform (FFT) of the ACF, expresses the relative weight of each roughness component of a surface structure as a function of its spatial frequency/wavelength. It describes the roughness power per unit frequency over the sampling length. The use of PSDF enables a more comprehensive characterization of structures and contains all the information about both the vertical and the lateral structural properties. The PSDF can be derived from surface profiles measured by an optical or mechanical profiler or from AFM surface profile data.

Previous work studied the correlation between superhydrophobicity and the PSDF of randomly rough surfaces and showed that superhydrophobic surfaces had a higher roughness power per unit frequency along the entire sampling length compared to non-superhydrophobic surfaces [45]. A surface containing both micro and nano roughness, will give a PSDF with higher roughness with small length scales (shorter than 500 nm) compared to a surface containing only micro or nano roughness [46]. Ice adhesion strength for superhydrophobic surfaces was found to be dependent primarily on the autocorrelation length [47]. The results suggested that surface features with small spacing are associated with a higher capillary pressure and better ability to resist a small droplet from physically penetrating into the space between the surface features.

Two parameters are extracted from PSDF that are of interest, they are the RMS roughness and the autocorrelation length [48]. The RMS roughness is related to height fluctuations and the autocorrelation length (ACL) is defined as a maximum distance over which significant correlation occurs, or the distance between two statistically independent points. Smoother surfaces generally have large correlation lengths, while rougher surfaces have low values of correlation lengths. More specifically, ACL describes the horizontal distance over which the surface profile is autocorrelated with a value larger than 1/e (0.368) [49]. Usually a rough surface corresponds to high values of RMS height and low values of ACL.

In spite of considerable work on superhydrophobic surfaces, there still remains a lack of knowledge on the specific roughness characteristics that lead to superhydrophobic coatings. Moreover, techniques to quantify the roughness of superhydrophobic surfaces are still needed. To reach this objective, in this work a variety of superhydrophobic and non-superhydrophobic surfaces were synthesized using identical nanosilica particles and fluorine chemistry, and various polymer binders on different substrates [50]. The resulting morphology was analyzed by a variety of experimental and statistical methods. Various parameters were used to study the role of feature roughness on superhydrophobicity, including common amplitude parameters comprised of Ra, RMS, kurtosis, and skewness, followed by statistical parameters such as ACL, and PSDF. The wide variety of the coating morphologies obtained allowed us to experimentally verify the theoretical models for the roughness factor and critical roughness parameters. It was found that the PSDF is a powerful tool for graphically predicting if a surface will be superhydrophobic. For the case of a man-made random surface morphologies, superhydrophobicity requires a tightly packed rough surface with an average peak radius in the micro and nanoscale smaller than 3 μm and 520 nm, respectively.

Experimental Methodology

A variety of surfaces were prepared using three different binders, nanosilica particles (NPs), and fluorosilane and their surface characteristics were studied with respect to their contact and sliding angles. To investigate the roughness effect on superhydrophobicity, the micro and nano roughness of the synthesized surfaces was investigated. Ra was calculated to elucidate whether a distinguishable Ra value can be obtained for superhydrophobic formulations compared to non-superhydrophobic ones. Then, the average radius and peak to peak distance were determined for all surfaces, using kurtosis and skewness calculations. The RMS and ACL were extracted to confirm if the surfaces were random Gaussian surfaces.

Materials and Methods

Fumed silica nanoparticles (CAB-O-SIL® TS-720 Cabot Corporation, USA) were used throughout the study. The particles were mixed with a fluoroalkylsilane (Dynasylan® F8263, Evonik, Germany) in isopropyl alcohol (IPA). The fluoroalkyl functionality provides low surface energy. The average particle (aggregate) diameter was 0.2-0.3 μm.

Three binders were used: ethyl cyanoacrylate resin (ECA) (Loctite® Super Glue, Henkel Corporation, USA), a two component epoxy (EPO-TEK® 301, Epoxy Technology, USA), and a one part ultraviolet (UV) curing urethane acrylate resin (UA) (NOA 61, Norland Products Incorporated, USA). The carrier solvent for the coating was acetone (Sigma Aldrich, USA).

The silica NPs (constant concentration of 2.5 wt %) were dispersed

in the fluoroalkylsilane solution (in isopropyl alcohol, (IPA)) and stirred at room temperature for 10 min. Each binder was dissolved in acetone and stirred for 10 min at room temperature. Then, the two solutions were mixed together and stirred for another 10 min. For each formulation, the binder concentration ranged from 5 to 25 wt % (in increments of 5%). A total of 15 formulations were prepared [50].

Coating

Glass microscope slides and polycarbonate (PC) sheet cut to 2.54 cm x 2.54 cm squares served as substrates for the coating. The substrates were rinsed with ethanol and dried under air pressure. One ml of solution was spin coated on the substrate at 1250 rpm for 1 minute. Ethyl cyanoacrylate and epoxy formulations were cured at 110 °C for 2 hours. Urethane acrylate was cured under UV radiation for 2 minutes. A medium pressure mercury lamp (Heraeus Noblelight America LLC) with a 365 nm wavelength at 100% intensity was used for the UV-curing.

Characterization

The contact angle was measured according to the sessile drop method using a commercial video-based, software-controlled, contact angle analyzer (DSA 100, KRUSS GmbH,Germany). Deionized water was used for the measurements. The sliding angle was measured using a tilting unit incorporated into the contact angle analyzer. A drop was first deposited on the horizontal substrate and after equilibrium the substrate plane was tilted until the onset of drop motion. Both contact and sliding angles were measured using a 5 µl water drop.

The profile of the surface was scanned using a stylus profilometer (DEKTAK, KRUSS GmbH,Germany). The stylus radius was 0.2 µm, the scan length 10 mm, and the scan time 120 sec.

Topography images were taken using Atomic Force Microscopy (AFM, PSIA XE-100) in noncontact mode. A scan size of 5X5 µm, with a scan rate of 0.5 Hz/sec was used and 256X256 pixel images were kept for all the samples.

Skewness and kurtosis were analyzed using two different software programs: XEI 100 (AFM PSIA 100 image analysis software) and Gwyddion 2.41 version (free software). The results of the two software programs were compared. The Power Spectral Density Function (PSDF) was extracted from AFM images using Gwyddion software.

The roughness factor (R_f) was calculated using Eq.1:

$$R_f = \sqrt{1 + 2\frac{\sigma^2}{l^2}\frac{1-exp(-l/\beta^*)^2}{\pi}} \quad \ldots\ldots\ldots 1$$

and the critical value of roughness factor (m_0) was calculated using Eq. 2:

$$m_0 = \left(\frac{\sigma}{l}\sqrt{\frac{1-[\exp(-\beta^*/l)]^2}{\pi}}\right) \ldots\ldots\ldots 2$$

where *l* is the sampling interval or short-wavelength limit, which is a distance between the measured data points, σ is the RMS roughness and β* is the ACL.

Results and Discussion

Contact and Sliding Angles

The superhydrophobicity of glass and PC substrates coated with silica NPs dispersed in different binders was evaluated by contact and sliding angle measurements. The weight ratio between binder and the NPs was varied and total of 30 formulations were prepared for coatings using the three binders coating on two substrates. Three samples were prepared for each formulation and the average values are shown in our previous work [51].

The contact angle measurements showed different results for the three binders on glass and PC. The effect of substrate and coating formulations on the resulting coatings' topographies were studied in our previous work [51]. It was shown that the interfacial tensions and spreading coefficients of the as prepared solutions and during the evaporation stage of the spin coating were the critical factors determining the localization of the NPs either on the surface or within the binder phase. The thermodynamic investigation was in good agreement with respect to the localization of the NPs as a function of the binder concentration and substrate type.

Amplitude Parameters Analysis

Microscopy and Profilometry Characterization

The localization of NPs on the top layer of the coating is a prerequisite for obtaining a superhydrophobic surface as it provides the needed nanoroughness [51]. However, not all surfaces with nanoroughness are superhydrophobic. Superhydrophobic surfaces require the correct micro and nanoroughness. To quantify the roughness effect on superhydrophobicity, the first section of this paper is directed toward analysis of the micro roughness and its variables, such as height (amplitude), and interval (wavelength). A 10 mm length scan was performed using a contact profilometer to calculate the average roughness, Ra. (The results are included in supporting section S1). As expected, Ra measurements alone did not show a clear distinction between superhydrophobic and non-superhydrophobic formulations. The results indicate that higher values of profile height are not essential for superhydrophobicity and most superhydrophobic formulations showed lower overall height (on glass and PC) compared to the non-superhydrophobic ones. The Ra parameter expresses the relative departure of the profile in the vertical direction, but does not provide any information about the slope, shapes, and sizes of the asperities or about the frequency and regularity of their occurrence [46] .

Profilometry Scans

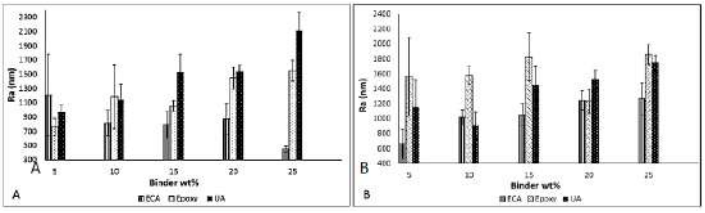

Figure S1: Ra roughness values of ECA, epoxy and UA formulations A) on glass B) on PC.

In order for a surface to show superhydrophobic characteristics, sharp structures having needle-like shapes with high aspect ratio and small spacing are needed to increase capillary pressure and trapped air [52]. Conversely, structures that have low projections cannot trap sufficient air and are not superhydrophobic. To provide detailed information on the microroughness surface structure with

varying binder wt %, a 500 µm scanned area was selected from the 10-mm scans. The surface profiles for all binder concentrations are included in the supporting section (S2-S4).

Profilometry Scans

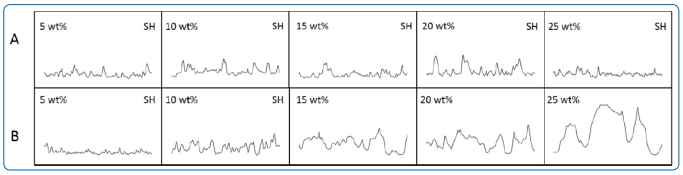

Figure S2: Surface structure for all ECA formulations A) on glass B) on PC (SH refers to superhydrophobic)

Profilometry Scans

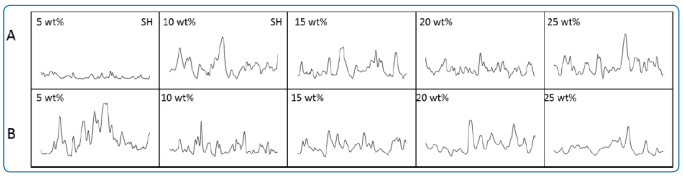

Figure S3: Surface structure for all epoxy formulations A) on glass B) on PC (SH refers to superhydrophobic)

Profilometry Scans

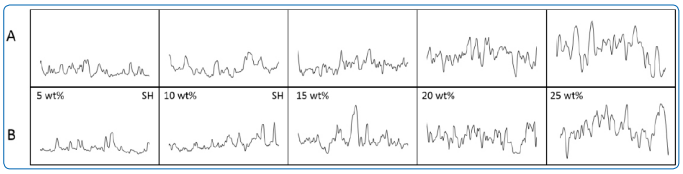

Figure S4: Surface structure for all UA formulations A) on glass B) on PC (SH refers to superhydrophobic)

The profilometer results indicate that sharp structures with high aspect ratio and small spacing (frequency) are needed for superhydrophobic surfaces to prevent water drops from penetrating between the peaks as opposed to the non-superhydrophobic surfaces. Comparison of microroughness profilometry results with NPs localization analysis from our previous study is presented in Tables 1-3. It shows that for ECA formulations NPs were seen on the surface a sharp (high aspect ratio) and packed (high packing density) topography was obtained for all the formulations on glass substrates. In the case of PC substrate, although NPs were seen on the surface, with increasing ECA wt %, the sharpness and the dense packing of the surface structure was lost, along with superhydrophobicity. The loss in sharpness was shown to be due to poor wetting of the ECA on the substrate that led to uncovered areas of the substrate with increasing binder concentration. For epoxy formulations on glass, sharpness and dense asperities were retained for all epoxy wt %, however, only 5 and 10 epoxy wt% were superhydrophobic since NPs were located on the surface. For PC, for all epoxy wt% sharpness and dense asperities were preserved, but the lack of correct nanoroughness (which cannot be determined by profilometry) did not produce superhydrophobicity. Urethane acrylate formulations exhibited sharp and dense structures on glass and PC, but only 5 and 10 UA wt % were superhydrophobic with NPs located on the surface. With increasing UA wt %, nanoroughness was lost due to penetration of the nanoparticles into the binder, resulting in loss of superhydrophobicity. From Tables 1-3 it can be determined that the presence of sharp and dense microroughness is not sufficient to predict superhydrophobicity or to characterize superhydrophobic surfaces comprising micro and nanoroughness, since it is limited to microroughness only.

Table 1: Profilometry Summary for ECA Based Formulations

Binder wt%	ECA					
	Glass			PC		
	Sharp	Dense	Superhydrophobic	Sharp	Dense	Superhydrophobic
5%	Y	Y	Y	Y	Y	Y
10%	Y	Y	Y	Y	Y	Y
15%	Y	Y	Y	N	N	N
20%	Y	Y	Y	N	N	N
25%	Y	Y	Y	N	N	N

Table 2: Profilometry Summary for Epoxy Based Formulations

Binder wt%	Epoxy					
	Glass			PC		
	Sharp	Dense	Superhydrophobic	Sharp	Dense	Superhydrophobic
5%	Y	Y	Y	Y	Y	N
10%	Y	Y	Y	Y	Y	N
15%	Y	Y	N	Y	Y	N
20%	Y	Y	N	Y	Y	N
25%	Y	Y	N	Y	Y	N

Table 3: Profilometry Summary for UA Based Formulations

Binder wt%	UA					
	Glass			PC		
	Sharp	Dense	Superhydrophobic	Sharp	Dense	Superhydrophobic
5%	Y	Y	Y	Y	Y	Y
10%	Y	Y	Y	Y	Y	Y
15%	Y	Y	N	Y	Y	N
20%	Y	Y	N	Y	Y	N
25%	Y	Y	N	Y	Y	N

Since nanoroughness was shown to be critical for superhydrophobicity, a detailed study of the coating's nanoroughness was carried out using AFM with a 20 µm scan length. AFM images for all formulations on glass and PC substrates are shown in SI 5-7.

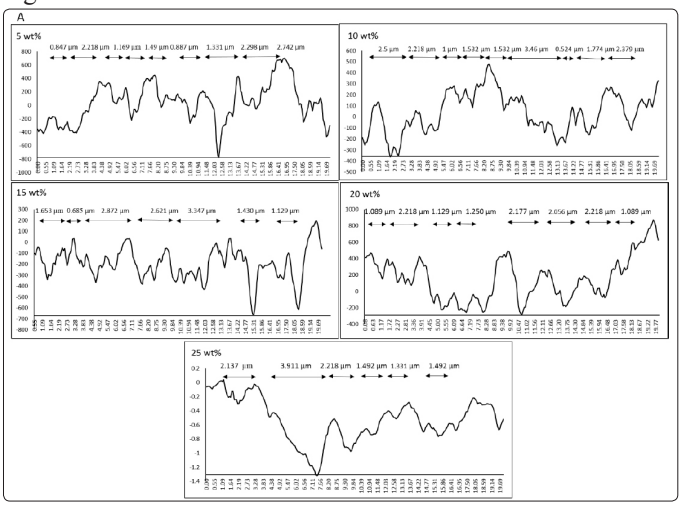

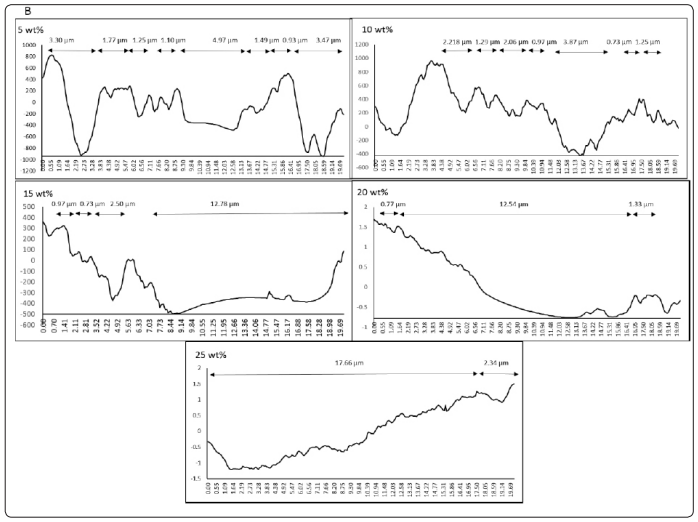

Figure S5. Surface profile of ECA formulations A) on glass B) on PC

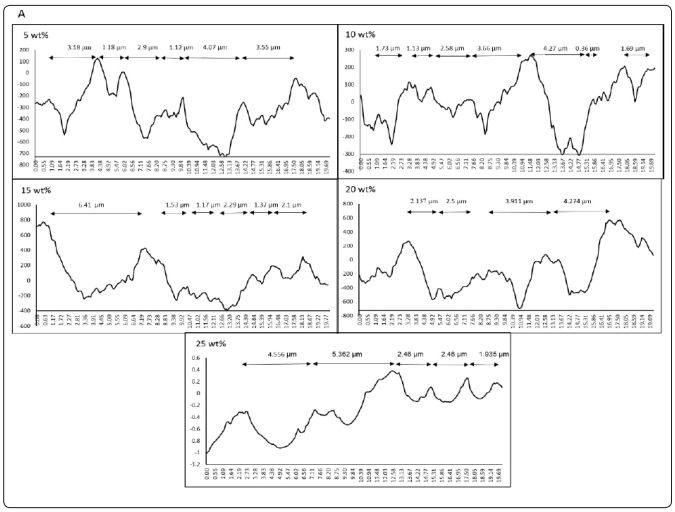

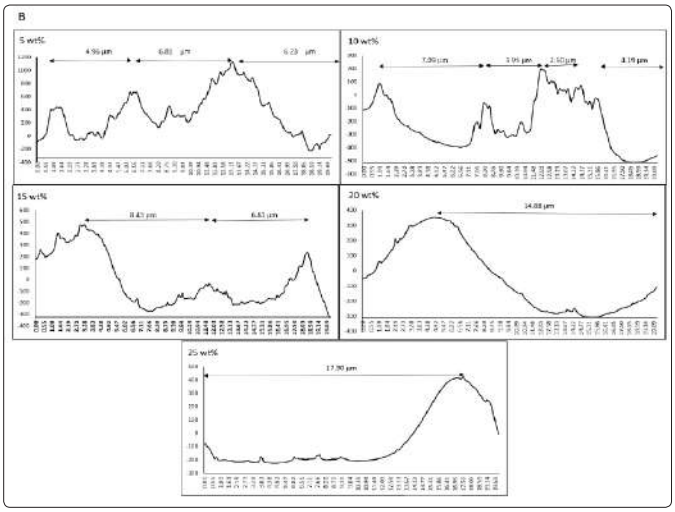

Figure S6: Surface profile of epoxy formulations A) on glass B) on PC.

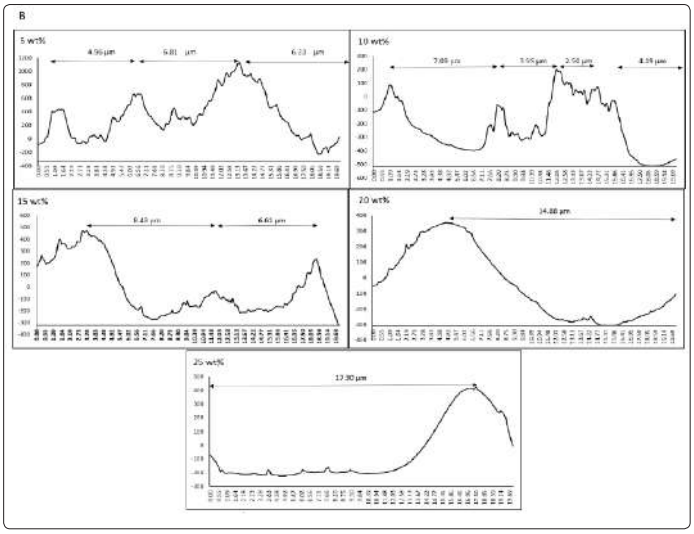

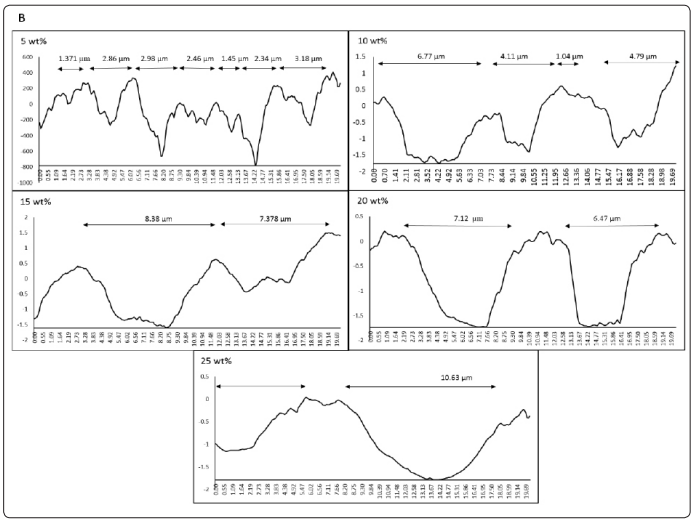

Figure S7: Surface profile of UA formulations A) on glass B) on PC

AFM topography images show the presence of NPs to different extents on the coated surfaces. In some formulations NPs cover the entire surface, and in some formulations they are mostly embedded in the coating [51]. Differences in surface structures were also observed when using other types of binders. (The surface profile was extracted from AFM images and results are shown in supporting section (S8-S10). A rigorous analysis of the surface profiles prepared by the different formulations, showed nanoroughness comprising of pyramidal asperities with a rounded tips in a few cases when coating glass. In the case of coating PC, the morphologies had hemispherical asperities with lower aspect ratios compared to the case of glass substrates. These results were in agreement with previous work on roughness of superhydrophobic surfaces where a preferable structure was shown to be comprised of pyramidal asperities with rounded tips [47].

The profiles were further analyzed for their average peak to peak distance and average peak radius. This was based on previous characterization for bio-inspired work on superhydrophobic leaves that exhibited characteristic average peak to peak distance and peak radius for the different leaves [51] .The average peak to peak distances for the synthesized formulations are given in Table 4.

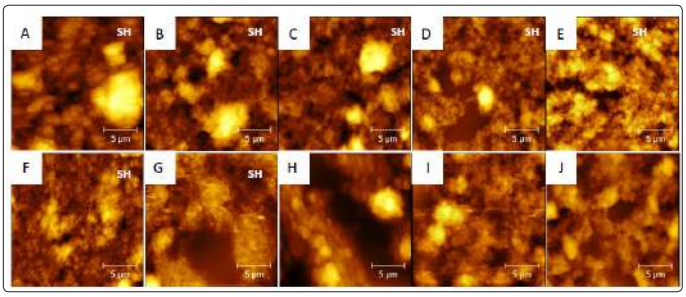

Figure S8: 20 µm AFM scan size of ECA A) 5 wt% B) 10 wt% C) 15 wt% D) 20 wt% E) 25wt% , on glass. F) 5 wt% G) 10 wt% H) 15 wt% I) 20 wt% J) 25wt% , on PC.

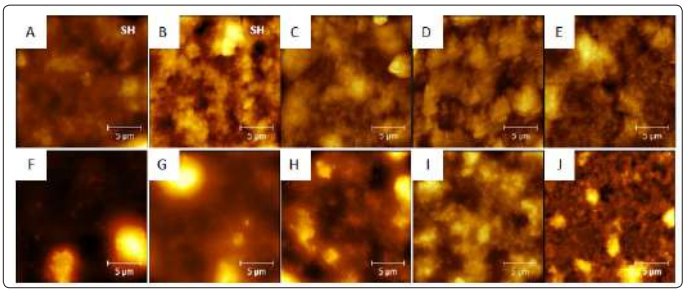

Figure S9: 20 µm AFM scan size of epoxy A) 5 wt% B) 10 wt% C) 15 wt% D) 20 wt% E) 25wt%, on glass. F) 5 wt% G) 10 wt% H) 15 wt% I) 20 wt% J) 25wt% , on PC.

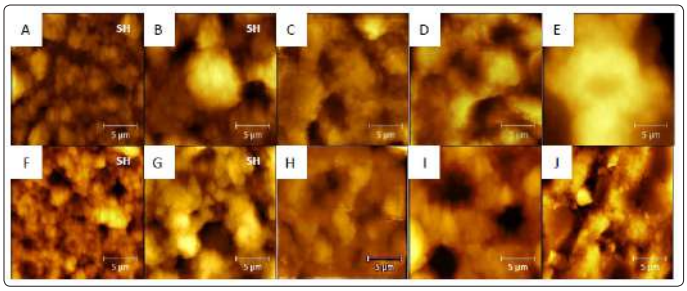

Figure S10: 20 µm AFM scan size of UA A) 5 wt% B) 10 wt% C) 15 wt% D) 20 wt% E) 25wt% , on glass. F) 5 wt% G) 10 wt% H) 15 wt% I) 20 wt% J) 25wt% , on PC.

Table 4: Average Peak to Peak Distance for All Formulations (SH refers to superhydrophobic)

Binder wt%	ECA		Epoxy		UA	
	Glass	PC	Glass	PC	Glass	PC
	Average (µm)	Average (µm)	Average (µm)	Average (µm)	Average (µm)	Average (µm)
5%	$1.62_{(SH)}$	$2.28_{(SH)}$	$2.60_{(SH)}$	1.82	$3.43_{(SH)}$	$2.54_{(SH)}$
10%	$1.88_{(SH)}$	$2.37_{(SH)}$	$2.51_{(SH)}$	5.08	$4.98_{(SH)}$	$4.17_{(SH)}$
15%	$1.96_{(SH)}$	12.78	5.65	7.52	8.04	7.88
20%	$1.52_{(SH)}$	12.54	3.20	15.00	7.42	6.79
25%	$2.09_{(SH)}$	17.66	3.35	17.00	>10.00	>10.00

The results in Table 4 indicate that all superhydrophobic formulations exhibit tightly packed structures as needed for superhydrophobicity with peak-to-peak distances shorter than 5 µm. The majority of non-superhydrophobic formulations show loosely packed structures, which may cause destabilization of the interface between the surface and the water drop and a loss of superhydrophobicity. A few non-superhydrophobic formulations, such as 20 and 25% epoxy on glass, exhibited average peak to peak distance below 5 µm, which shows that peak to peak distance is only one topography requirement for superhydrophobicity. In addition to the peak to peak distance, the other parameter to be analyzed is the average peak radius, which is shown in Table 5.

Table 5: Average Peak Radius Values for All Formulations (SH refers to superhydrophobic)

Binder wt%	ECA		Epoxy		UA	
	Glass	PC	Glass	PC	Glass	PC
	Average (µm)	Average (µm)	Average (µm)	Average (µm)	Average (µm)	Average (µm)
5%	$0.35_{(SH)}$	$0.30_{(SH)}$	$0.23_{(SH)}$	0.79	$0.22_{(SH)}$	$0.32_{(SH)}$
10%	$0.31_{(SH)}$	$0.31_{(SH)}$	$0.42_{(SH)}$	0.95	$0.33_{(SH)}$	$0.26_{(SH)}$
15%	$0.32_{(SH)}$	0.31	0.36	1.26	0.93	2.00
20%	$0.45_{(SH)}$	>5.00	1.09	1.51	1.16	2.20
25%	$0.44_{(SH)}$	>5.00	1.05	1.62	1.35	>5.00

The observed results show that for all superhydrophobic formulations, the average peak radius was below 0.5 µm, which is smaller than the typical droplet size. It should be noted that a few formulations showed an average peak radius below 1 µm with no superhydrophobicity, but in those cases the surfaces did not have a peak-to-peak distance shorter than 5 µm. Table 5 also explains why the 20 and 25% epoxy on glass samples did not show superhydrophobicity since they did not have average peak radii less than 0.5 µm. Thus, one requirement for superhydrophobicity is a peak to peak distance of less than 5 µm and a peak radius below 0.5 µm. However, our previous results51 and in general, for superhydrophobic surfaces characterization of the average peak to peak distance and peak radius at the microscale are not sufficient to predict superhydrophobicity [53-55]. Statistical parameters such as skewness and kurtosis were calculated to further characterize the surfaces. The two parameters were calculated using two different software programs (XEI and Gwyddion) for the 20 µm scan size to study the asymmetry of pillar heights and peakedness or bluntness of the surfaces. For reference, the skewness and kurtosis for dry lotus leaves were also calculated and their values were 0 and 3 respectively [46]. The results are shown in Tables 6-8.

Table 6: Skewness (Sk) and Kurtosis (Ku) Values for ECA Formulations (SH refers to superhydrophobic)

ECA		XEI		Gwyddion	
		Sk	Ku	Sk	Ku
	$5\%_{(SH)}$	0.06	3.01	0.03	2.94
	$10\%_{(SH)}$	-0.45	3.41	0.49	3.05
Glass	$15\%_{(SH)}$	-0.12	2.77	0.85	2.88
	$20\%_{(SH)}$	0.24	3.22	0.78	3.06
	$25\%_{(SH)}$	-0.81	2.92	0.42	2.80
	$5\%_{(SH)}$	-0.66	5.18	-0.05	2.38
	$10\%_{(SH)}$	-0.42	3.13	0.04	2.45
PC	15%	0.01	2.49	0.97	3.44
	20%	0.48	4.22	0.23	2.24
	25%	0.26	2.16	0.85	2.98

Table 7: Skewness (Sk) and Kurtosis (Ku) Values for Epoxy Formulations
(SH refers to superhydrophobic)

Epoxy		XEI		Gwyddion	
		Sk	Ku	Sk	Ku
	5% (SH)	-0.25	2.45	0.58	2.79
Glass	10% (SH)	-0.14	2.99	-0.19	3.03
	15%	-0.52	4.22	-0.23	2.38
	20%	-0.49	2.75	0.12	2.56
	25%	-0.20	3.31	0.30	2.26
	5%	-1.83	7.23	0.64	2.89
	10%	-0.16	3.00	0.00	2.47
PC	15%	-0.02	3.28	0.55	2.47
	20%	-1.00	4.14	0.60	2.15
	25%	0.06	2.64	0.53	2.32

Table 8: Skewness (Sk) and Kurtosis (Ku) Values for UA Formulations
(SH refers to superhydrophobic)

UA		XEI		Gwyddion	
		Sk	Ku	Sk	Ku
	5% (SH)	-0.68	4.02	0.33	2.75
	10% (SH)	-0.40	3.65	0.22	2.98
Glass	15%	-0.72	2.98	-0.24	2.92
	20%	0.36	3.17	-0.10	2.52
	25%	0.34	2.75	-0.15	2.01
	5% (SH)	-0.44	4.36	0.16	2.99
	10% (SH)	0.33	2.42	-0.05	2.63
PC	15%	0.10	2.54	-0.13	2.48
	20%	0.40	2.58	0.04	2.46
	25%	0.73	4.22	-0.24	2.30

As can be concluded from the results, the skewness and kurtosis values did not vary much between the two software programs. All surfaces, both superhydrophobic and non-superhydrophobic, showed nearly Gaussian distribution values similar to the dry lotus leaf indicating roughly similar numbers of hills and valleys (Sk values close to 0.0) with more blunt topography (Ku values close to 3.0). Hence, a random surface roughness (superhydrophobic and non-superhydrophobic) with a Gaussian distribution is produced by spin coating. Additionally, the Tables show that the skewness and kurtosis values do not provide information to predict superhydrophobicity in a coating since all samples show similar values. The fact the surfaces are Gaussian permits the use of the power spectrum density function to extract parameters to characterize the roughness [56].

Power Spectrum Density Function (PSDF) of Surfaces

The dry lotus leaf, which can be used as a model for the necessary characteristics of a superhydrophobic surface, possesses both micro and nanoscale roughness. Consequently, the PSDF was analyzed for both the dry lotus leaf and the engineered surfaces. Both a microroughness and nanoroughness study were carried using PSDF. The significance of the PSDF is that it provides information over the entire range of length scales as opposed to characterization of a single set of values. This is particularly important for random Gaussian surfaces where there is not the level of control over the aspect ratio and sizes as in surfaces created with periodic defined structures.

Microroughness Parameters

Starting with microroughness, PSDFs for all the 20 µm scan sizes were computed and are shown in Figure 1. Blue curves are indicative of superhydrophobic surfaces (contact angle above 150°), while red curves are for non superhydrophobic surfaces (contact angles below 150°). The black curve shows the dried lotus leaf for comparison. Figure 1 shows the PSDF (Amplitude at different wavelengths) for all the surfaces and the dry lotus leaf at the micron scale.

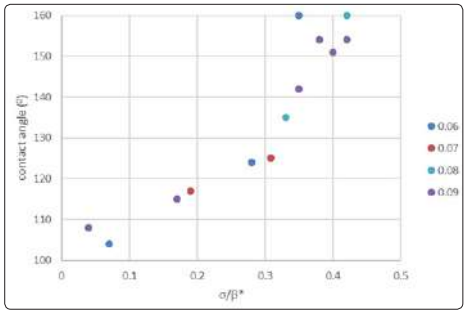

Figure 1: PSDFs for all formulations on glass and PC

The graphs show the logarithm of the PSD of surface roughness plotted versus the logarithm of the length scale, or in other words the graph describes the mean surface roughness at each length scale in a given image.

A close analysis of the PSDF curves indicate that most superhydrophobic and non-superhydrophobic plots (except for Epoxy 10-25 wt% on PC) overlap each other indicating a similar spectral microroughness range. Since it has been shown previously that larger spectral roughness (high spectral strength) at long wavelength regions represents the aggregates, we can say that the presence of micro aggregates is not enough to indicate a superhydrophobic structure [57]. RMS and ACL values for all surfaces were extracted from the PSDF plots and are shown in supporting information S11.

Table S11 : RMS and ACL for all formulations on glass and PC. 20 µm scan size. Bold values for superhydrophobic surfaces

Dry Lotus				ECA		Epoxy		UA	
RMS	ACL			RMS	ACL (µm)	RMS	ACL	RMS	ACL
		Glass	5%	0.28	0.74	0.44	1.08	0.29	0.69
			10%	0.23	0.68	0.19	0.73	0.49	0.95
			15%	0.38	0.82	0.62	1.48	0.61	1.54
			20%	0.38	0.85	0.44	1.43	0.49	1.98
			25%	0.33	0.93	0.53	2.69	0.67	2.35
		PC	5%	0.36	0.65	0.18	1.21	0.32	0.67
			10%	0.29	0.70	0.22	1.91	0.66	0.80
			15%	0.37	1.25	0.24	1.61	0.50	1.73
			20%	N/A	N/A	0.28	1.57	0.92	1.12
			25%	N/A	N/A	0.10	1.54	0.32	1.32

The results show lower range of ACL for all superhydrophobic formulations indicating tightly packed asperities. All non

superhydrophobic formulations exhibited higher range of ACL indicating less packed asperities. ECA 20 and 25 wt% on PC were not analyzed because our previous SEM micrographs showed the presence of coated and non-coated regions on the PC for high ECA concentrations with coated areas exhibiting superhydrophobicity and uncoated areas that were non-superhydrophobic [51]. Thus, these formulations were not included in the analysis. As opposed to ACL, no significant trend was observed in RMS values for superhydrophobic surfaces. This is probably due to the high scanning range size and lack of accuracy in scanning nanoscale features, which is a necessary size range for superhydrophobicity. Thus, to study the nanoroughness it was necessary to reduce the scan size to 5 µm.

Nanoroughness Characterization

AFM images for all the formulations on glass and PC, as well as for dry lotus, are shown in SI 12-15. PSDFs are given for all the formulations in Figure 2.

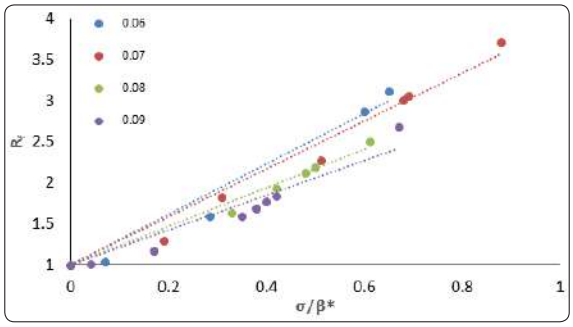

Figure 2: Power spectral density as a function of wavelength for all formulations on glass and on PC

PSDF results show that all superhydrophobic surfaces (blue curves) exhibit larger spectral roughness (high spectral strength) at long wavelength regions, while non-superhydrophobic surfaces show lower spectral strength than the dry lotus at the longer wavelengths. At short wavelengths all superhydrophobic surfaces have higher spectral strength than the dry lotus. At short wavelengths (nanoscale) four non-superhydrophobic surfaces (epoxy 20% on glass, epoxy 10% on PC, UA 15% on glass and on PC) also had spectral strength higher than the dry lotus, however, they did not show spectral roughness at the long wavelength that was equal or greater than the dry lotus. Thus, using the dry lotus as a guide to the overall roughness required for superhydrophobicity we can see that both micro and nanoscale roughness is required. The results also indicate the importance of having sufficient micron scale roughness (long wavelength) for superhydrophobicity and that the amount can be quantified graphically. Thus, the use of the PSDF enables the characterization of the entire spectrum of sizes and can be used to determine if the characteristics of the surface will provide superhydrophobicity. Numerical values of RMS and ACL were also extracted from PSD curves and the results are shown in supporting information S16.

Table S16: RMS and ACL values extracted from PSDF results. 5 µm AFM scan size. Bold values are for superhydrophobic surfaces

Dry Lotus				ECA		Epoxy		UA	
RMS	ACL			RMS (nm)	ACL (nm)	RMS (nm)	ACL (nm)	RMS (nm)	ACL (nm)
120	330	Glass	5%	153	227	121	250	218	336
			10%	136	268	146	202	127	254
			15%	157	199	82	214	146	394
			20%	240	273	97	247	71	190
			25%	200	291	81	353	56	288
		PC	5%	193	155	74	210	143	234
			10%	109	152	83	163	197	329
			15%	95	227	39	227	89	224
			20%	N/A	N/A	10	224	89	224
			25%	N/A	N/A	21	301	89	313

A statistical approach has been used previously to model the contact between multiple-asperities and showed that for a random surface with a certain σ (RMS rou8hness) and β*(ACL), the average peak radius, R_p is defined by [58]:

$$R_p \propto \frac{(\beta^*)^2}{\sigma}$$

The calculated values for R_p in the microscale range are shown in Table 9 and the nanoscale range in Table 10.

Table 9: Calculated values for Rp (micron scale)

		ECA	Epoxy	UA
		Rp (µm)	Rp (µm)	Rp (µm)
	5%	1.95 (SH)	2.65 (SH)	1.64 (SH)
	10%	2.01 (SH)	2.80 (SH)	1.84 (SH)
Glass	15%	1.77 (SH)	3.53	3.89
	20%	1.90 (SH)	4.65	8.00
	25%	2.62 (SH)	13.65	8.247
	5%	1.17(SH)	8.13	1.40 (SH)
	10%	1.69 (SH)	16.58	0.97 (SH)
PC	15%	4.22	10.80	5.98
	20%	3.4	8.80	1.36
	25%	2.51	23.71	5.44

Table 10: Calculated values for Rp (nanoscale)

		ECA	Epoxy	UA
		Rp (nm)	Rp (nm)	Rp (nm)
Glass	5%	336.79 (SH)	516.53 (SH)	517.87 (SH)
	10%	528.12 (SH)	279.48 (SH)	508 (SH)
	15%	252.24 (SH)	558.49	1063.26
	20%	310.54 (SH)	628.96	508.45
	25%	423.40 (SH)	1538.38	1481.14
PC	5%	124.48 (SH)	595.95	382.91 (SH)
	10%	211.96 (SH)	320.11	549.44 (SH)
	15%	542.41	1321.26	563.77
	20%	N/A	5017.6	765.11
	25%	N/A	4314.33	1100.77

Our results show that all superhydrophobic surfaces had average peak radius in the micro and nanoscale smaller than 3 µm and 520 nm, respectively. It should be noted that the statistical results for average peak radius were greater than the measured values (Table 5) but still low compared to the non superhydrophobic surfaces. These results are consistent with a previous study on the lotus leaf with average peak radius of 3 to 4 µm (dried or fresh) and 100 to 150 nm at the micro and nanoscale, respectively [59]. The results show that random surfaces created using a polymer composite, exhibiting a quantifiable surface structure similar to superhydrophobic biological surfaces, will also show superhydrophobicity. The surfaces should have packed asperities (peak to peak distance below 5 µm) together with small peak radii the micro and nanoscale to distinguish superhydrophobic from non superhydrophobic surfaces.

A previous theoretical study related the roughness factor (RMS/ACL ratio) for different sampling interval (l)/ACL ratio of a random surface roughness having a Gaussian distribution [60]. A critical value of the roughness parameters [mo = tan(-θ0)] was used to define the transition from the Wenzel to the Cassie-Baxter state. It was found that for most natural and engineered materials with Guassian roughness, the ratio RMS/ACL should be much smaller than 0.1 and the critical value of the roughness parameters (m_0) (equation 2) should be much smaller than 1 [60]. Using the large number of surfaces generated in this work to experimentally verify this theory, (all have Gaussian distribution (with skewness≈0 and kurtosis≈3)) the roughness factor and critical value of roughness parameters for all surfaces were calculated together with the absolute slope value. All samples were divided to groups by their different sampling interval (l)/ ACL ratio. θ_0 is the contact angle for the flat surface of ECA, epoxy and UA coated with FAS having the values of 110o, 115 o, 110 o respectively. The calculated results are shown in supporting information SI 17.

Table S17: Contact angle (CA), RMS/ACL ratio (σ / β*), roughness factor (Rf) and critical value of the roughness parameter (mo) for all formulations divided by their sampling interval/ ACL ratio (l/β*)

l/β*	Formulation	CA	σ / β*	Rf	mo
0.05	UA 15% on glass	151	0.37	2.09	8.14
0.06	Epoxy 25% on PC	104	0.07	1.04	2.47
	UA 25% on PC	124	0.28	1.6	3.27
	Dry Lotus	160	0.35	2.72	-
	UA 10% on PC	160	0.6	2.87	3.27
	UA 5% on glass	160	0.65	3.12	8.14
0.07	UA25% on PC	117	0.19	1.29	3.27
	Epoxy 25% on glass	125	0.308	1.82	1.96
	ECA 10% on glass	160	0.51	2.28	5.67
	ECA 5% on PC	160	0.19		2.47
	ECA 25% on glass	160	0.308	1.82	5.67
	ECA 20% on glass	160	0.51	2.28	5.67
0.08	ECA 20% on PC	135	0.68	3.01	3.27
	ECA 10% on glass	160	0.69	3.06	3.15
	Epoxy 5% on glass	160	0.88	3.72	1.96
	UA 10% on Glass	160	0.5	2.2	8.14
	UA 5% on PC	160	0.61	2.5	3.27
0.09	Epoxy 20% on PC	108	0.04	1.01	2.47
	Epoxy 15% on PC	115	0.17	1.18	2.47
	Epoxy 5% on PC	142	0.35	1.6	2.47
	Epoxy 15% on glass	154	0.38	1.69	1.96
	UA 15% on PC	151	0.4	1.77	3.27
	ECA 15% on PC	154	0.42	1.84	2.47
	ECA 5% on glass	160	0.67	2.68	5.67
0.10	UA 20% on glass	123	0.37	1.6	8.14
	Epoxy 20% on glass	135	0.39	1.82	1.96
	Epoxy 10% on glass	160	0.72	2.69	1.96
	ECA 15% on glass	160	0.79	2.89	5.67
0.12	Epoxy 10% on PC	123	0.51	1.86	2.47
0.13	ECA 20% on PC	130	0.34	1.42	2.47
	ECA 25% on PC	130	0.45	1.70	2.47

The calculated critical values of the roughness parameters (m_0), as shown in SI17, were in good agreement with the theory that contact angle may approach superhydrophobicity (≥160) prior to reaching the critical values of the roughness parameter (for example 20 and 25 wt% ECA on glass).

The relationship between roughness factor and RMS/ACL is presented in Figure 3 using Eq. 1 and the dependence of the contact angle on RMS/ACL is presented in Figure 4. Due to a lack of data points for few sampling interval/ ACL ratios, Figures 3 and 4 include the dependence of roughness factor to RMS/ACL for sampling interval/ACL of 0.06, 0.07, 0.08, and 0.09 only.

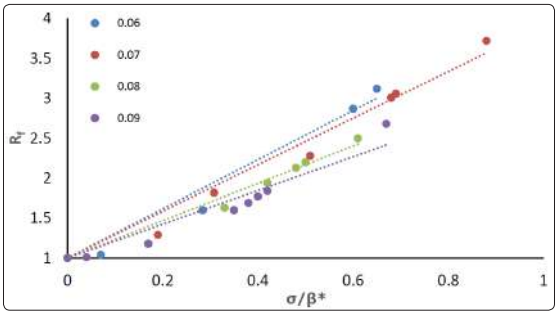

Figure 3: Roughness factor (R_f) as function of RMS/ACL ratio (σ / β*) for Gaussian surfaces for different sampling interval/ACL values

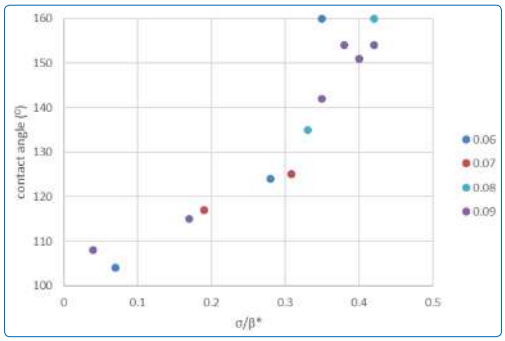

Figure 4: Contact angle as function of RMS/ACL ratio (σ / β*) for Gaussian surfaces for different sampling interval/ACL values

The results are consistent with previous work that both the roughness factor and the contact angle increase with increasing RMS/ACL and these engineered surfaces fit the theoretical models [60]. In contrast, the RMS/ACL results for the present engineered Gaussian surfaces, however, show that for realistic values of RMS/ACL (i.e. RMS/ACL> 0.1) it is possible to achieve high contact angles.

Of critical interest for designing surfaces is the result that surfaces must have RMS/ACL values of 0.35 or higher in order to provide superhydrophobicity. This corresponds to a roughness value of ~2 (Figure 3) to achieve superhydrophobicity in these systems.

Conclusion

This research was focused on understanding and quantifying the role of roughness for random Gaussian superhydrophobic coatings. Thirty different surface structures were prepared and studied comprising three different binders, five different binder/NPs ratio on two substrates with different wetting characteristics (hydrophilic and hydrophobic). The surfaces were analyzed by AFM for peak to peak distances and average radius. It was found that superhydrophobic surfaces require a peak to peak distance below 5 microns and a radius of less than 0.5 micron, however, this is not sufficient to predict or characterize superhydrophobic surfaces. The surfaces were also analyzed using two different data analysis programs. Skewness and kurtosis for all the surfaces were determined and showed that the engineered coatings had a random Gaussian roughness distribution, but there was no significant difference in the skewness and kurtosis values for either superhydrophobic or non-superhydrophobic surfaces. The power spectral density function (PSDF) was found to be an effective tool to study the roughness needed for superhydrophobicity. Comparison with the PSDF for a dry lotus leaf provided distinction between superhydrophobic and non superhydrophobic surfaces. Both RMS roughness and ACL were determined from PSDF of the AFM scans for the coatings and compared to a dry lotus leaf. The results showed that the ACL for all superhydrophobic formulations were in the micron and submicron range indicating that tightly packed asperities are essential for superhydrophobicity. The significance of the PSDF is that it provides information over the entire range of length scales as opposed to characterization of a single set of values. This is particularly important for random Gaussian surfaces where there is not the level of control over the aspect ratio and sizes as is surfaces created with defined structures (such as in periodic lithographic patterning).

The average peak radius for the micro and nano scales calculated from ACL and RMS values were found to be less than 3 μm and 520 nm respectively. The results support the accepted theory is that superhydrophobic surfaces require tightly packed asperities and small micron and nano roughness.

The surfaces were found to fit theoretical models for the roughness factor and critical roughness parameters, providing experimental verification. The accepted theory is that superhydophic surfaces require both micron and nano roughness. In this work, the results indicated that surfaces required both a critical distance and radius for superhydrophobicity. It was found that the RMS/ACL values should be 0.35 or higher for designing surfaces with contact angles above 150o. The work presented here provides a critical tool for measuring, quantifying, and understanding the role of roughness for a range of superhydrophobic surface applications. Ultimately, the results can be used to design surfaces for superhydrophobicity. As such, it gives a much needed methodology to quantify surface structures for applications such as self-cleaning, icephobicity, anti-biofouling, corrosion resistance, and water repellency.

Aknowledgements

The authors would like to thank the support of the National Science Foundation (Award #EEC-0832785) and the Davis and Francis Pernick Fund.

References

1. Rios PF, Dodiuk H, Kenig S, Mccarthy S, Dotan A (2008) Durable ultra-hydrophobic surfaces for self-cleaning applications 1684-1691.
2. Wisdom KM, Watson Ja, Qu X, Liu F, Watson GS, et al. (2013) Self-cleaning of superhydrophobic surfaces by self-propelled jumping condensate. Proc Natl Acad Sci U S A 110: 7992-7997.
3. Blossey R (2003) Self-cleaning surfaces--virtual realities. Nat Mater 2: 301–306
4. Dodiuk H, Rios PF, Dotan A, Kenig S, Gan R (2007) Hydrophobic and self-cleaning coatings 746-750.
5. Liu K, Cao M, Fujishima A, Jiang L (2014) Bio-Inspired Titanium Dioxide Materials with Special Wettability and Their Applications. Chem Rev.
6. Gould P (2003) Smart , clean surfaces 44-48.
7. Chen Y, Chen S, Yu F, Sun W, Zhu H,et al. (2009) Fabrication and anti-corrosion property of superhydrophobic hybrid film on copper surface and its formation mechanism. Surf Interface Anal 41: 872-877.
8. She Z, Li Q, Wang Z, Li L, Chen F, et al. (2013) Researching the fabrication of anticorrosion superhydrophobic surface on magnesium alloy and its mechanical stability and durability. Chem Eng J 228: 415-424.
9. Howarter J, Youngblood JP (2008) Self-Cleaning and Next Generation Anti-Fog Surfaces and Coatings. Macromol Rapid Commun 29: 455-466.
10. Ming Z, Jian L, Chunxia W, Xiaokang Z, Lan C (2011) Fluid drag reduction on superhydrophobic surfaces coated with carbon nanotube forests (CNTs). Soft Matter 7: 4391-4396.
11. Dong H, Cheng M, Zhang Y, Wei H, Shi F (2013) Extraordinary drag-reducing effect of a superhydrophobic coating on a macroscopic model ship at high speed. J Mater Chem A 1: 5886-5891.
12. Lee M, Yim C, Jeon S (2014) Characterization of underwater stability of superhydrophobic surfaces using quartz crystal microresonators. Langmuir 30: 7931-7935.
13. Mazumder P, Jiang Y, Baker D, Carrilero A, Tulli D, et al. (2014) Superomniphobic, Transparent, and Antireflection Surfaces Based on Hierarchical Nanostructures . Nano Lett 14: 4677-4681.
14. Hejazi V, Sobolev K (2013) Nosonovsky M. From superhydrophobicity to icephobicity: forces and interaction analysis. Sci Rep 3: 2194.
15. Petrenko V (2003) Study of The Physical Mechanisms of Ice Adhesion 387: 81.
16. Dotan A, Dodiuk H, Laforte C, Kenig S (2009) The Relationship between Water Wetting and Ice Adhesion. J Adhes Sci Technol 1907-1915.
17. Alizadeh A, Yamada M, Li R, Shang W, Otta S, et al. (2012) Dynamics of ice nucleation on water repellent surfaces. Langmuir 28: 3180-3186.

18. Mishchenko L, Hatton B, Bahadur V, Taylor JA, Krupenkin T,et al. (2010) Design of Ice-free Nanostructured Impacting Water Droplets 4: 7699-7707.
19. Kulinich S, Farhadi S, Nose K, Du XW (2011) Superhydrophobic surfaces: are they really ice-repellent? Langmuir 27: 25-29.
20. Farhadi S, Farzaneh M, Kulinich S (2011) Anti-icing performance of superhydrophobic surfaces. Appl Surf Sci 257: 6264-6269.
21. Du LU, Chicoutimi QÀ, Partielle CE, Maîtrise DELA, Ingénierie EN (2010) Water and ice-repellent properties of nanocomposite coatings based on silicone rubber Propriétés hydrophobes et glaciophobes de revêtements nanocomposites à base de silicone.
22. Wang F, Lv F, Liu Y, Li C, Lv Y (2013) Ice adhesion on different microstructure superhydrophobic aluminum surfaces. J Adhes Sci Technol 27: 58-67.
23. Zimmermann J, Reifler F, Fortunato G, Gerhardt L-C, Seeger S (2008) A Simple, One-Step Approach to Durable and Robust Superhydrophobic Textiles. Adv Funct Mater 18: 3662-3669.
24. Zhao Y, Xu Z, Wang X, Lin T (2012) Photoreactive azido-containing silica nanoparticle/polycation multilayers: durable superhydrophobic coating on cotton fabrics. Langmuir 28: 6328-6335.
25. Nahum T, Dodiuk H, Dotan A, Kenig S, Paul Lellouche J (2014) Superhydrophobic durable coating based on UV-photoreactive silica nanoparticles. J Appl Polym Sci 41122.
26. Puretskiy N, Stoychev G, Synytska A, Ionov L (2012) Surfaces with self-repairable ultrahydrophobicity based on self-organizing freely floating colloidal particles. Langmuir 28: 3679-3682.
27. Xiu Y, Liu Y, Hess DW, Wong CP (2010) Mechanically robust superhydrophobicity on hierarchically structured Si surfaces. Nanotechnology 21: 155705.
28. Verho T, Bower C, Andrew P, Franssila S, Ikkala O, et al. (2011) Mechanically durable superhydrophobic surfaces. Adv Mater 23: 673-678.
29. Bhushan B, Jung YC, Koch K (2009) Micro-, nano- and hierarchical structures for superhydrophobicity, self-cleaning and low adhesion. Philos Trans A Math Phys Eng Sci 367: 1631-1672.
30. Yang C, Tartaglino U, Persson B (2006) Influence of Surface Roughness on Superhydrophobicity. Phys Rev Lett 97: 116103.
31. Ma Z, Jiang C, Li X, Ye F, Yuan W (2013) Controllable fabrication of periodic arrays of high-aspect-ratio micro-nano hierarchical structures and their superhydrophobicity. J Micromechanics Microengineering 23: 095027.
32. Schulte AJ, Droste DM, Koch K, Barthlott W (2011) Hierarchically structured superhydrophobic flowers with low hysteresis of the wild pansy (Viola tricolor) - new design principles for biomimetic materials. Beilstein J Nanotechnol 2: 228-236.
33. Moradi S, Englezos P, Hatzikiriakos SG (2014) Contact angle hysteresis of non-flattened-top micro/nanostructures. Langmuir 30: 3274-3284.
34. Rios PF, Dodiuk H, Kenig S, McCarthy S, Dotan A (2006) The effects of nanostructure and composition on the hydrophobic properties of solid surfaces. J Adhes Sci Technol 20: 563-587.
35. Bhushan B, Jung YC (2008) Wetting, adhesion and friction of superhydrophobic and hydrophilic leaves and fabricated micro/nanopatterned surfaces. J Phys Condens Matter 20: 225010.
36. Zhang B, Wang J, Zhang X (2013) Effects of the Hierarchical Structure of Rough Solid Surfaces on the Wetting of Microdroplets. Langmuir.
37. Cao F, Guan Z, Li D (2008) Preparation of material surface structure similar to hydrophobic structure of lotus leaf. J Wuhan Univ Technol Sci Ed 23: 513–517.
38. Huang Y, Sarkar DK, Chen X-G (2010) A one-step process to engineer superhydrophobic copper surfaces. Mater Lett 64: 2722-2724.
39. Yoon Y, Lee D-W, Lee J-B (2012) Surface modified nano-patterned SU -8 pillar array optically transparent super-hydrophobic thin film. J Micromechanics Microengineering 22: 035012.
40. Wooh S, Koh JH, Lee S, Yoon H, Char K (2014) Trilevel-Structured Superhydrophobic Pillar Arrays with Tunable Optical Functions. Adv Funct Mater.
41. Li X, Tay BK, Miele P, Brioude A, Cornu D (2009) Fabrication of silicon pyramid/nanowire binary structure with superhydrophobicity. Appl Surf Sci 255: 7147-7152.
42. Xiu Y, Zhu L, Hess DW, Wong CP (2007) Hierarchical silicon etched structures for controlled hydrophobicity/superhydrophobicity. Nano Lett 7: 3388-3393.
43. Bhushan B, Petralia P (2013) Tribology in Practice Series: Principles and Applications to Tribology. John Wiley & Sons.
44. Kulinich SA, Farzaneh M (2009) " How Wetting Hysteresis Influences Ice Adhesion Strength on Superhydrophobic Surfaces", Langmuir 25: 8854-8856.
45. Awada H, Grignard B, Jerome C, Vaillant A, Coninck JD, et al. (2010) " Correlation between Superhydrophobicity and the Power Spectral Density of Randomly Rough Surfaces", Langmuir 26: 17798-17803.
46. Dhillon PK, Brown PS, Bain CD, Badyal JP, Sakar S (2014) "Topographobical length scales of hierarchical superhydrophobic surfaces", Applied surface science 317: 1068-1074.
47. Yeong YH (2015) Milionis A., and Loth E. " Atmospheric Ice Adhesion on Water-Repellent Coatings: Wetting and Surface Topology Effects", Langmuir 31: 13107-13116.
48. Janusz J "Description of Topography of Surfaces and Thin Films with the use Fourier Transformation, Obtained from Non-Standard Optical Measurements", Institute of Physics, Cracow University of Technology.
49. Gupta VK, Jangir A (2011) "Microwave response of rough surfaces with auto-correlation functions, RMS heights and correlation lengths using active remote sensing", Indian Journal of Radio & Space Physics 40: 137-146.
50. Nahum T, Dodiuk H, Kenig S, Panwar A, Barry C, et al. (2017) " The effect of Composition and Thermodynamic on the Surface Morphology of Durable Superhydrophobic Polymer Coatings", Nanotechnology, Science and Applications 10.
51. Schulte AJ, Droste DM, Koch K, Barthlott W (2011) "Hierarchically structured superhydrophobic flowers with low hysteresis of the wild pansy (Viola tricolor) – new design principles for biomimetic materials". Beilstein Journal of Nanotechnology 2: 228-236.
52. Teisala H, Tuominen M, Kuusipalo J (2011) "Adhesion Mechanism of Water Droplets on Hierarchically Rough Superhydrophobic Rose Petal Surface". Journal of Nanomaterials.
53. Bixler GD,Bhushan B (2015) "Rice and Butterfly Wing Effect Inspired Low Drag and Antifouling Surfaces: A Review", Critical Reviews in Solid State and Materials Sciences 40: 1-37.
54. Burton Z, Bhushan B (2006) "Surface characterization and

adhesion and friction properties of hydrophobic leaf surfaces", Ultramicroscopy 106: 709-719.
55. Bhushan B (2012) "Biomimetics: Bioinspired Hierarchical-Structured Surfaces for Green Science and Technology" Springer Science & Business Media.
56. Nosonovsky M, Bhushan B (2008) " Biologically Inspired Surfaces: Broadening the Scope of Roughness" Adv. Funct. Mater 18: 843-855.
57. Senthilkumar M, Sahoo NK, Thakur S, Tokas RB (2005) " Characterization of microroughness parameters in gadolinium oxide thin films: A study based on extended power spectral density analyses", Applied Surface Science 252: 1608–1619.
58. Bhushan B, Nosonovsky M (2004) "Scale effects in dry and wet friction, wear, and interface temperature" Nanotechnology 15: 749-761.
59. Bhushan B, Jung YC (2008) "Wetting, adhesion and friction of superhydrophobic and hydrophilic leaves and fabricated micro/nanopatterned surfaces" Journal of Physics Condensed Matter 20: 225010.
60. Nosonovsky M, Bhushan B (2005) " Roughness optimization for biomimetic superhydrophobic surfaces" Microsyst Tehhnol 11: 535-549.

SUPPORTING INFORMATION

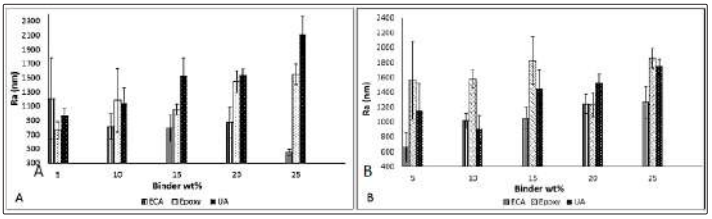

Figure S1. Ra roughness values of ECA, epoxy and UA formulations A) on glass B) on PC.

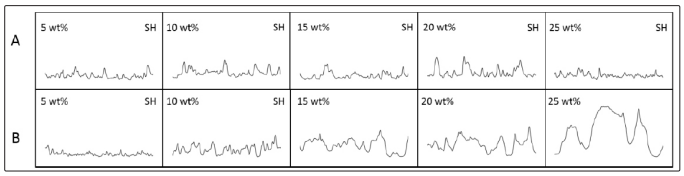

Figure S2: Surface structure for all ECA formulations A) on glass B) on PC (SH refers to superhydrophobic)

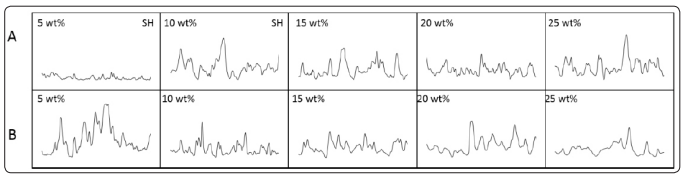

Figure S3: Surface structure for all epoxy formulations A) on glass B) on PC (SH refers to superhydrophobic)

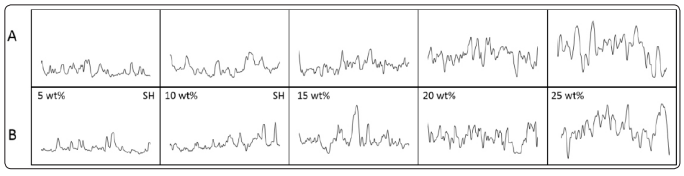

Figure S4: Surface structure for all UA formulations A) on glass B) on PC (SH refers to superhydrophobic)

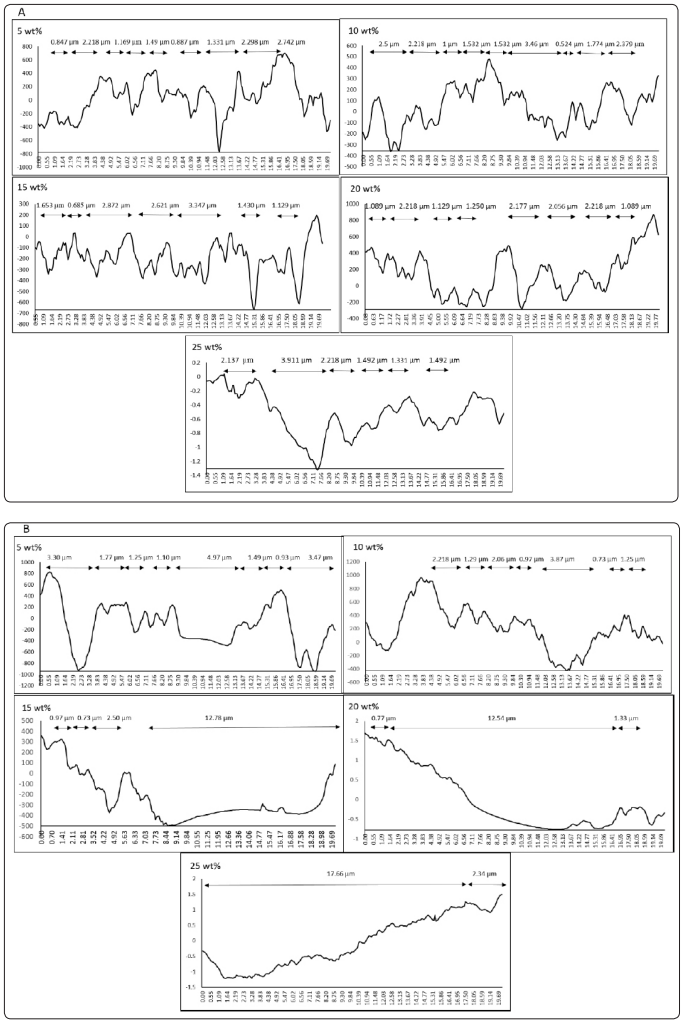

Figure S5. Surface profile of ECA formulations A) on glass B) on PC

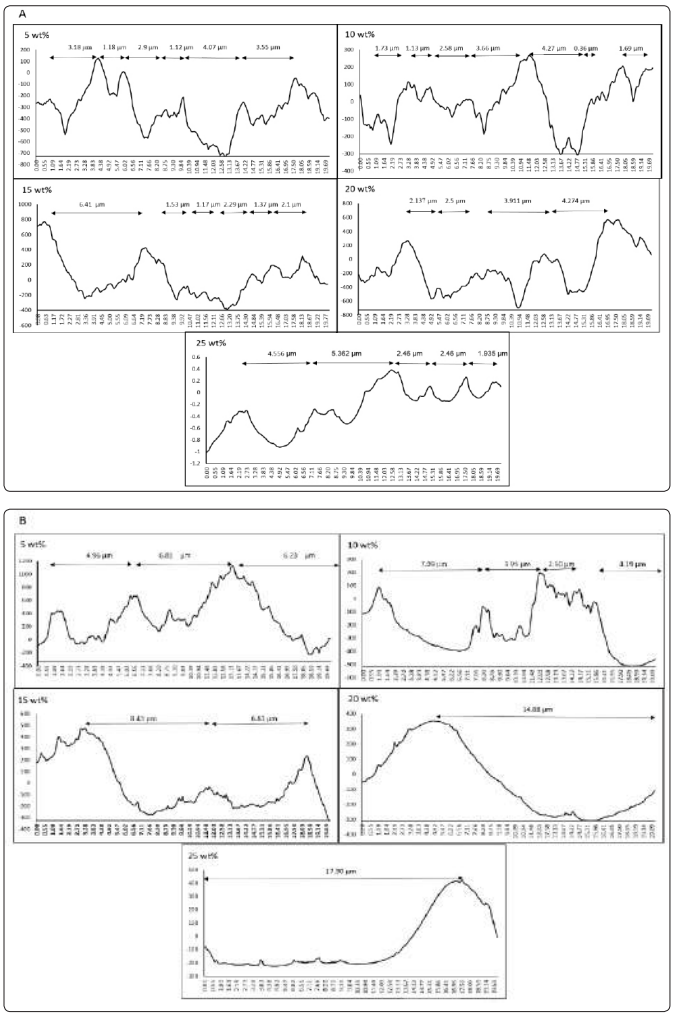

Figure S6. Surface profile of epoxy formulations A) on glass B) on PC

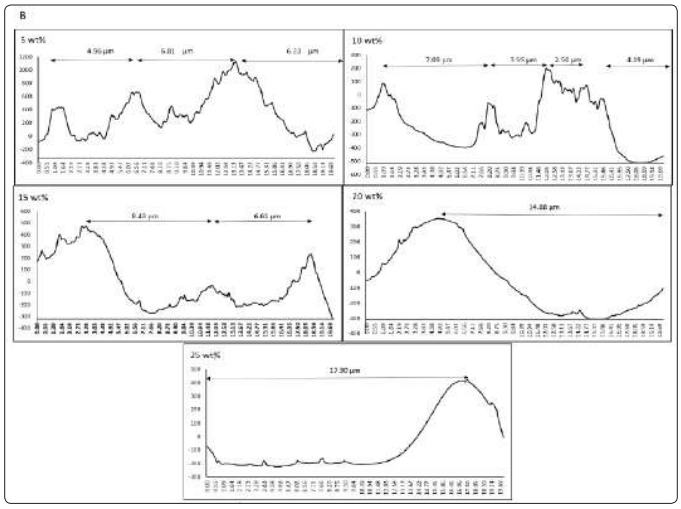

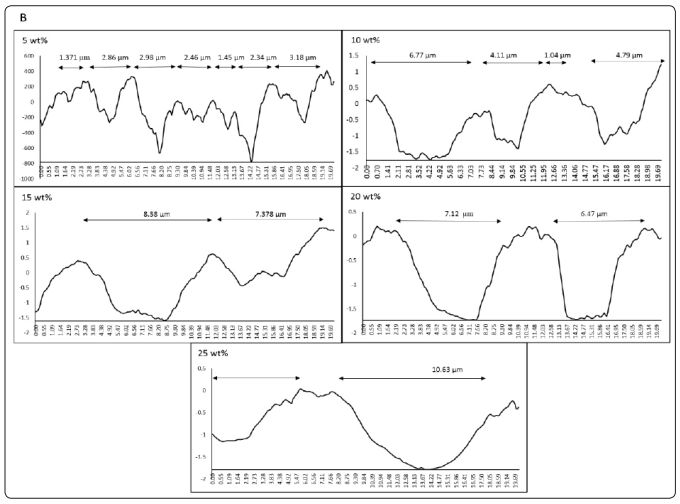

Figure S7: Surface profile of UA formulations A) on glass B) on PC

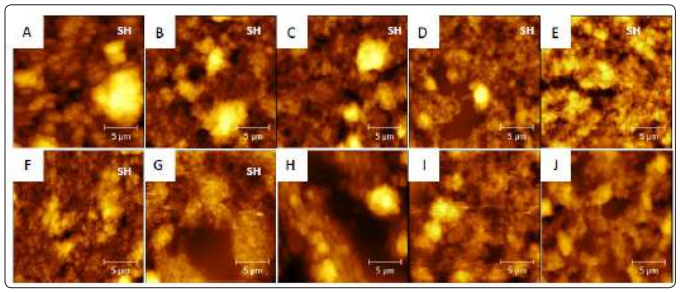

Figure S8: 20 µm AFM scan size of ECA A) 5 wt% B) 10 wt% C) 15 wt% D) 20 wt% E) 25wt% , on glass. F) 5 wt% G) 10 wt% H) 15 wt% I) 20 wt% J) 25wt% , on PC

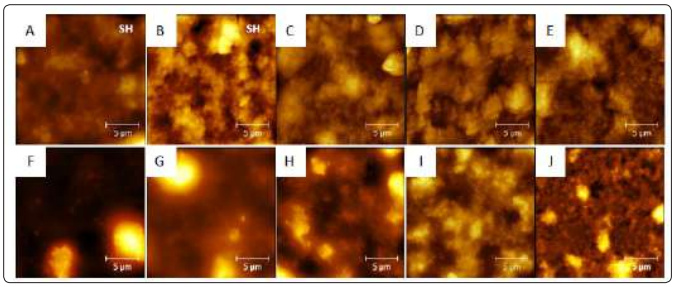

Figure S9: 20 µm AFM scan size of epoxy A) 5 wt% B) 10 wt% C) 15 wt% D) 20 wt% E) 25wt%, on glass. F) 5 wt% G) 10 wt% H) 15 wt% I) 20 wt% J) 25wt% , on PC

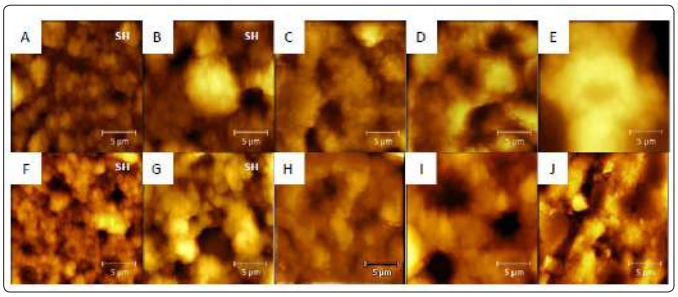

Figure S10: 20 µm AFM scan size of UA A) 5 wt% B) 10 wt% C) 15 wt% D) 20 wt% E) 25wt% , on glass. F) 5 wt% G) 10 wt% H) 15 wt% I) 20 wt% J) 25wt% , on PC.

Table S11 : RMS and ACL for all formulations on glass and PC. 20 µm scan size. Bold values for superhydrophobic surfaces

Dry Lotus				ECA		Epoxy		UA	
RMS	ACL			RMS	ACL (µm)	RMS	ACL	RMS	ACL
		Glass	5%	0.28	0.74	0.44	1.08	0.29	0.69
			10%	0.23	0.68	0.19	0.73	0.49	0.95
			15%	0.38	0.82	0.62	1.48	0.61	1.54
			20%	0.38	0.85	0.44	1.43	0.49	1.98
			25%	0.33	0.93	0.53	2.69	0.67	2.35
		PC	5%	0.36	0.65	0.18	1.21	0.32	0.67
			10%	0.29	0.70	0.22	1.91	0.66	0.80
			15%	0.37	1.25	0.24	1.61	0.50	1.73
			20%	N/A	N/A	0.28	1.57	0.92	1.12
			25%	N/A	N/A	0.10	1.54	0.32	1.32

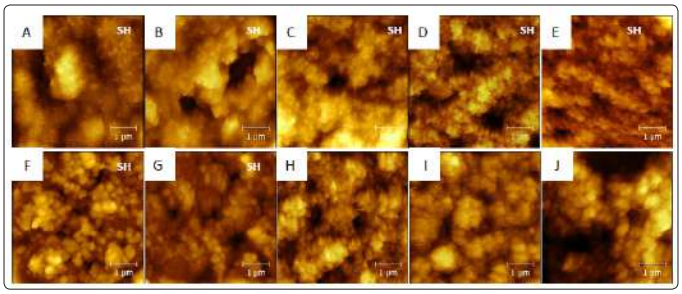

Figure S12: 5 µm AFM scan size of ECA A) 5 wt% B) 10 wt% C) 15 wt% D) 20 wt% E) 25wt%, on glass. F) 5 wt% G) 10 wt% H) 15 wt% I) 20 wt% J) 25wt% , on PC

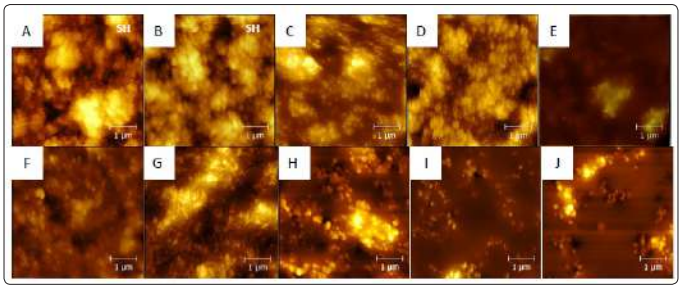

Figure S13: 5 µm AFM scan size of epoxy A) 5 wt% B) 10 wt% C) 15 wt% D) 20 wt% E) 25wt% , on glass. F) 5 wt% G) 10 wt% H) 15 wt% I) 20 wt% J) 25wt% , on PC

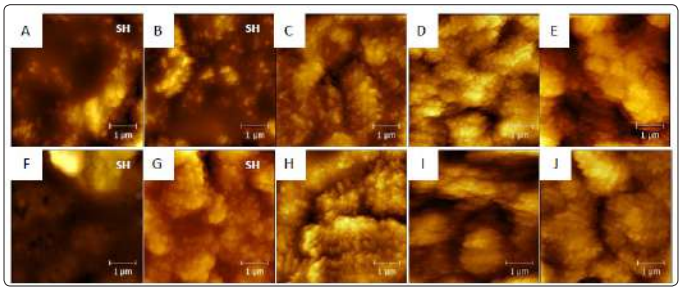

Figure S14: 5 µm AFM scan size of UA A) 5 wt% B) 10 wt% C) 15 wt% D) 20 wt% E) 25wt%, on glass. F) 5 wt% G) 10 wt% H) 15 wt% I) 20 wt% J) 25wt% , on PC

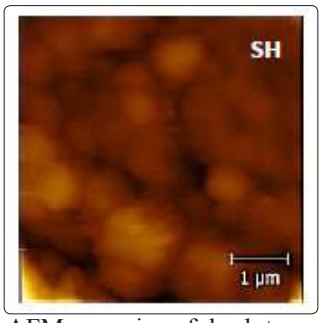

Figure S15: 5 µm AFM scan size of dry lotus

Table S16: RMS and ACL values extracted from PSDF results. 5 µm AFM scan size. Bold values are for superhydrophobic surfaces

Dry Lotus				ECA		Epoxy		UA	
RMS	ACL			RMS (nm)	ACL (nm)	RMS (nm)	ACL (nm)	RMS (nm)	ACL (nm)
120	330	Glass	5%	153	227	121	250	218	336
			10%	136	268	146	202	127	254
			15%	157	199	82	214	146	394
			20%	240	273	97	247	71	190
			25%	200	291	81	353	56	288
		PC	5%	193	155	74	210	143	234
			10%	109	152	83	163	197	329
			15%	95	227	39	227	89	224
			20%	N/A	N/A	10	224	89	224
			25%	N/A	N/A	21	301	89	313

Table S17: Contact angle (CA), RMS/ACL ratio (σ / β*), roughness factor (Rf) and critical value of the roughness parameter (mo) for all formulations divided by their sampling interval/ ACL ratio (l/β*)

l/β*	Formulation	CA	σ / β*	Rf	mo
0.05	UA 15% on glass	151	0.37	2.09	8.14
0.06	Epoxy 25% on PC	104	0.07	1.04	2.47
	UA 25% on PC	124	0.28	1.6	3.27
	Dry Lotus	160	0.35	2.72	-
	UA 10% on PC	160	0.6	2.87	3.27
	UA 5% on glass	160	0.65	3.12	8.14
0.07	UA25% on PC	117	0.19	1.29	3.27
	Epoxy 25% on glass	125	0.308	1.82	1.96
	ECA 10% on glass	160	0.51	2.28	5.67
	ECA 5% on PC	160	0.19		2.47
	ECA 25% on glass	160	0.308	1.82	5.67
	ECA 20% on glass	160	0.51	2.28	5.67
0.08	ECA 20% on PC	135	0.68	3.01	3.27
	ECA 10% on glass	160	0.69	3.06	3.15
	Epoxy 5% on glass	160	0.88	3.72	1.96
	UA 10% on Glass	160	0.5	2.2	8.14
	UA 5% on PC	160	0.61	2.5	3.27

0.09	Epoxy 20% on PC	108	0.04	1.01	2.47
	Epoxy 15% on PC	115	0.17	1.18	2.47
	Epoxy 5% on PC	142	0.35	1.6	2.47
	Epoxy 15% on glass	154	0.38	1.69	1.96
	UA 15% on PC	151	0.4	1.77	3.27
	ECA 15% on PC	154	0.42	1.84	2.47
	ECA 5% on glass	160	0.67	2.68	5.67
0.10	UA 20% on glass	123	0.37	1.6	8.14
	Epoxy 20% on glass	135	0.39	1.82	1.96
	Epoxy 10% on glass	160	0.72	2.69	1.96
	ECA 15% on glass	160	0.79	2.89	5.67
0.12	Epoxy 10% on PC	123	0.51	1.86	2.47
0.13	ECA 20% on PC	130	0.34	1.42	2.47
	ECA 25% on PC	130	0.45	1.70	2.47